

Very high contrast integral field spectroscopy of AB Doradus C: 9-mag contrast at 0.2 arcsec without a coronagraph using spectral deconvolution†

Niranjan Thatte,^{1★} Roberto Abuter,^{2★} Matthias Tecza,^{1★} Eric L. Nielsen,^{3★} Fraser J. Clarke^{1★} and Laird M. Close^{3★}

¹*Department of Astrophysics, Denys Wilkinson Building, Keble Road, Oxford OX1 3RH*

²*Max-Planck-Institut für extraterrestrische Physik & European Southern Observatory, D-85748 Garching, Germany*

³*Steward Observatory, University of Arizona, Tucson, AZ 85721, USA*

Accepted 2007 March 8. Received 2007 March 8; in original form 2006 June 6

ABSTRACT

We present an extension of the spectral deconvolution (SD) method to achieve very high contrast at small inner working radii. We apply the method to the specific case of ground-based adaptive optics fed integral field spectroscopy (without a coronagraph). Utilizing the wavelength dependence of the Airy and speckle patterns, we make an accurate estimate of the point spread function that can be scaled and subtracted from the data cube. The residual noise in the resulting spectra is very close to the photon noise from the starlight halo. We utilize the technique to extract a very high signal-to-noise ratio *H*- and *K*-band spectrum of AB Doradus (AB Dor) C, the low-mass companion to AB Dor A. By effectively eliminating all contamination from AB Dor A, the extracted spectrum retains both continuum and spectral features. The achieved 1σ contrast is 9 mag at 0.2 arcsec, 11 mag at 0.5 arcsec, in 20 min exposure time, at an effective spectral bandwidth of 5.5 nm, proving that the method is applicable even in low-Strehl regimes.

The SD method clearly demonstrates the efficacy of image slicer based integral field units in achieving very high contrast imaging spectroscopy at small angular separations, validating their use as high-contrast spectrographs/imagers for extreme adaptive optics systems.

Key words: instrumentation: adaptive optics – instrumentation: spectrographs – binaries: close – stars: individual: AB Doradus C – stars: low-mass, brown dwarfs.

1 INTRODUCTION

Direct imaging and spectroscopy of extrasolar planets is a research area that has attracted significant attention in recent years. Several specialized instruments are now being designed and built to achieve this goal within the next few years [e.g. Keck XAOPI – Macintosh et al. 2004; VLT Planet Finder (SPHERE) – Beuzit et al. 2006; Gemini GPI – Soummer et al. 2006]. The major difficulty in detecting exoplanets is the extreme contrast between the star (typically a main-sequence M–G dwarf) and the planet (typically less than 1 arcsec away). Even in the most-favourable conditions, theoretical computations (e.g. Burrows, Sudarsky & Hubeny 2004) have shown

that the brightness ratio between the parent star and the exoplanet is expected to be at least 15 mag at 1 arcsec. Such contrasts are significantly beyond normal imaging techniques even with the best adaptive optics systems available today. If we are to attain this ambitious goal, novel ways to maximize the achieved contrast must be devised.

Even in high-Strehl adaptive optics (AO) systems, long exposures do not provide a smooth halo around the central star, as one would expect from a time-average of the speckles caused by atmospheric turbulence. In fact, due to the presence of super-speckles, imaging contrasts are much worse than the theoretical *photon noise* limit (Racine et al. 1999). Super-speckles (also called quasi-static speckles, Marois et al. 2006) are long-lived speckles caused by imperfections in the light path, and have coherence times ranging from tens of seconds to several minutes. Any changes in the light path, for example, due to instrument flexure or changing telescope position, cause the super-speckles to vary, making it impossible to remove them with static calibrations obtained at a different time [e.g. point spread function (PSF) star observations will show a completely different super-speckle pattern].

*E-mail: thatte@astro.ox.ac.uk (NT); rabuter@eso.org (RA); mtecza@astro.ox.ac.uk (MT); enielsen@as.arizona.edu (ELN); fclarke@astro.ox.ac.uk (FJC); lclose@as.arizona.edu (LMC)

†Based on observations collected at the European Southern Observatory (ESO), Chile, under ESO programme 276.C-5013.

The contrast limitations posed by super-speckles can only be overcome through *simultaneous* observations. Several techniques have been proposed to achieve this (e.g. Guyon 2004; Marois et al. 2004, 2006; Ren & Wang 2006) including the ‘spectral difference imager’ (SDI) technique developed by one of the authors (Lenzen et al. 2004) and others (Marois et al. 2005). The technique utilizes the fact that the planetary spectrum has sharp, deep absorption features (e.g. CH₄ in the *H* band) to dramatically improve the contrast with respect to scattered starlight, which has a smooth spectrum. By taking simultaneous images in and out of the methane absorption band, and scaling and subtracting the two images, one effectively removes the starlight, while leaving the planetary light intact. The subtraction removes residual starlight, whether in the form of rapidly time-varying speckles, slowly varying super-speckles, or any other form of scattered light within the telescope and instrument. In fact, the SDI technique uses an ingenious double-difference, so as to further reduce any residuals arising from systematic errors due to differing optical paths. Biller et al. (2006) have demonstrated the success of SDI in finding cool companions with the NACO instrument on the ESO-VLT.

SDI is, however, limited in application as it relies on an intrinsic feature of the companion spectrum; the CH₄ absorption feature only found in objects with $T_{\text{eff}} < 1200$ K. In addition, there is a need for follow-up spectroscopy of the candidate object detected – both to confirm its nature (often via common proper motion with the parent) and to characterize it in detail. In this paper, we describe an extension of the Sparks & Ford (2002) *spectral deconvolution* (SD) technique to achieve high-contrast imaging (and spectroscopy) with an integral field spectrograph (IFS). This technique does not rely on any feature of the target object’s spectrum and is therefore applicable to any high-contrast imaging application. In addition, the use of an IFS provides a complete data set in one go, and with maximum signal-to-noise ratio (S/N) (no slit losses). Furthermore, complete 2D spatial information allows the continuum to be correctly measured, in contrast to extremely narrow slits needed for AO-assisted spectroscopy. No a priori information about the spatial location of the companion is needed either, an inherent advantage of using an IFS.

Section 2 describes the Sparks & Ford (2002) method, as well as proposed extensions, including using this technique at small inner working radii (within the bifurcation radius, see Section 2.2), and in Section 3 we provide a demonstration of the achievable performance in this regime, *even without a coronagraph*. Section 3.4 presents the results and Section 4 elaborates on the future prospects and the discovery potential for high-contrast imaging spectroscopy with image slicer based IFSs, utilizing this technique.

2 CONCEPT

Several authors (e.g. Sparks & Ford 2002; Fusco et al. 2005; Berton et al. 2006) have suggested that the wealth of spectral information available in an IFS data cube can be utilized to remove scattered starlight and identify the presence of a close-in companion, and extract its spectrum with enhanced S/N, thus maximizing contrast. Our scheme is an extension of the SD technique proposed by Sparks & Ford (2002), adapted to ground-based observing with both extreme adaptive optics and general-purpose adaptive optics systems, and further optimized to maximize S/N. An application of the concept to ground-based IFS fed by general-purpose AO systems is very challenging, as the Strehl ratio is typically only ~ 0.5 , and varies strongly with wavelength.

The central tenet of the SD technique is that the position of almost all features arising from the parent star (Airy pattern, speckles, etc.) scales smoothly and slowly with wavelength (e.g. the first Airy null is always $1.22 \lambda/D$ from the star), whereas a physical object’s location is independent of wavelength. Thus, stepping through the wavelength axis of an IFS data cube at a fixed spatial location (e.g. the location of a companion), one would see a modulation arising from maxima and minima of the Airy pattern passing through the companion’s location (see fig. 24 in Sparks & Ford 2002). These modulations would drown out any expected signal from the companion. If, however, we use the wavelength dependence to advantage, we can effectively subtract all wavelength-dependent artefacts in the stellar PSF, thus unmasking the presence of real physical objects.

The technique is best illustrated via the removal of the Airy pattern from the IFS data cube, although it applies equally well to any *achromatic* aberration in the wavefront. Each wavelength slice of the IFS data cube is scaled radially, so as to exactly compensate the wavelength dependence of the Airy pattern. Nulls and maxima in the Airy pattern, which used to be located at different radial distances in the different wavelength slices now line up perfectly at all wavelengths in the scaled data cube (e.g. fig. 27 in Sparks & Ford 2002). The companion’s light now traces a diagonal line through the data cube.

Sparks & Ford (2002) fit a low-order polynomial to every spatial pixel (spaxel¹) of the data cube, while rejecting outliers. The result is a very high-S/N estimate of the Airy pattern (and all wavelength-dependent speckles) at each wavelength of the data cube. The faint companion represents a high frequency modulation and is thus excluded from the low-order polynomial fit (as it represents a tilted line through the scaled data cube, it is present in any given spaxel over only a small range of wavelengths). The light from the parent star is then subtracted from each scaled slice of the data cube, and the result scaled back to the original grid, to form the result cube.

The actual implementation of the concept for ground-based AO-assisted integral field spectroscopic data (without a coronagraph) has to account for low Strehl that varies substantially with wavelength. Furthermore, we have extended the original concept in two ways: (i) to extract spectra from objects that lie close to the parent star and (ii) optimize the S/N of the extracted spectra. We elaborate on these extensions in the following sections.

2.1 Application to faint companions at small separations

The SD technique utilizes the wavelength dependence of PSF features to obtain a high-S/N estimate of the parent star PSF, while rejecting the light from the faint companion. We first derive the limiting distance for which the technique is applicable in its original proposed form, and then explain how we deal with close-in companions.

2.2 Bifurcation point for characterization analysis

Consider a companion object located at radial distance r (expressed in angular units) from the primary object, imaged with a telescope of diameter D . The distance to the first null of the Airy pattern is given by the usual formulation

$$\Theta_0 = 1.22 \frac{\lambda_0}{D}, \quad (1)$$

¹ The term spaxel describes all pixels spanning the entire wavelength range of an IFS data cube that correspond to a single spatial pixel.

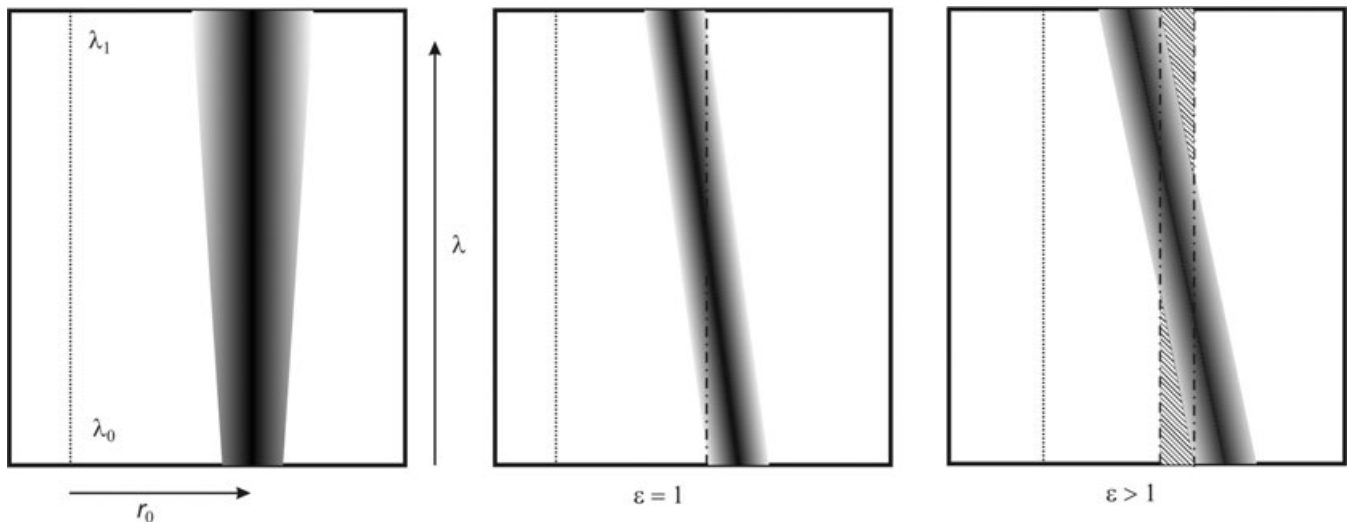


Figure 1. The left-hand panel is a schematic of a slice through the IFU data cube, in the x - λ plane, with the x -axis along the line joining the centre of the star with the centre of the faint companion. The dotted line represents the peak of the stellar light profile (as a function of λ). The size of the companion, quantified as $2.44\lambda/D$, increases with wavelength. The middle panel shows the data cube scaled inversely with wavelength, centred on the star. The faint companion’s separation is such that $\epsilon = 1$. The collapsed cube will be contaminated by companion light at all r values. The right-hand panel illustrates the situation for $\epsilon > 1$, where the hatched areas represent parts of the data cube not contaminated by light from the companion. It is thus possible to create a collapsed image free from companion light.

where λ_0 is the shortest wavelength in the IFU data cube. Defining the object extent as equal to $2\Theta_0$, and the wavelength range of the IFU as extending from λ_0 (shortest) to λ_1 (longest), we obtain an expression for the movement of the companion’s centre in the scaled data cube as

$$\Delta r = r - r \frac{\lambda_0}{\lambda_1} = r \frac{\Delta\lambda}{\lambda_1}. \quad (2)$$

Noting that the extent of the object stays constant in the scaled data cube, we can then express the bifurcation point as

$$\Delta r = r \frac{\Delta\lambda}{\lambda_1} = 2\epsilon \times 1.22 \frac{\lambda_0}{D}, \quad (3)$$

where ϵ is a factor slightly greater than 1. The parameter ϵ is explained in Fig. 1.

For $\epsilon \equiv 1$, the scaled data cube is entirely contaminated by light from the companion, but only just so. For $\epsilon > 1$, a *clean* collapsed image devoid of flux from the companion object can be made by collapsing a small fraction of wavelength channels at either end of the data cube. This is only necessary in the near vicinity of the faint companion, as shown by the hatched areas in the right-hand panel of Fig. 1.

The amount by which ϵ must exceed unity depends on the S/N of the observation, as sufficient number of wavelength channels must be used to form the high-S/N PSF estimate. Table 1 lists values of the bifurcation point for typical near-infrared band passes for an 8-m telescope, for a couple of typical values of ϵ . It is obvious from the table that extended wavelength coverage by the IFU is crucial for removing the flux from a close-in companion in the scaled data cube.

2.3 Extension to close-in faint companions

We have extended the SD technique to close-in faint companions by using an iterative technique to remove the faint companion’s light from the PSF estimate made using the scaled data cube. Residual light from the faint companion in the estimated PSF will reduce the

Table 1. Bifurcation point in the data reduction as a function of bandpass of observations and factor ϵ . r is the value of the bifurcation radius in milliarcseconds.

Band	λ_1 (μm)	λ_2 (μm)	ϵ	r (mas)
<i>H</i>	1.45	1.8	1.1	516
<i>K</i>	1.95	2.45	1.1	661
<i>H + K</i>	1.45	2.45	1.1	246
<i>H</i>	1.45	1.8	1.2	563
<i>K</i>	1.95	2.45	1.2	721
<i>H + K</i>	1.45	2.45	1.2	268

flux level of the companion in the final result cube. Furthermore, due to the wavelength-scaling process, any residual light will affect spectral channels differently, resulting in an error in the continuum slope of the derived faint companion spectrum. Section 3 shows that both the total flux and the continuum slope were correctly measured for the observations reported here, thus proving the efficacy of the proposed extension to the SD technique.

The following assumes that the position of the close-in faint companion is already known (Section 3.4 mentions how this might be derived from the IFU data cube itself). The companion is also assumed to be an unresolved point source, with a full width at half-maximum (FWHM) roughly equal to the diffraction-limited FWHM for the telescope aperture in question.

Knowing both the position and the size of the source, we fit for the companion amplitude and background level in individual spectral channels of the observed data, prior to scaling. Subtracting an ideal Airy pattern centred on the primary improves the robustness of the fit, as does averaging ~ 10 spectral channels. Scatter in the fit parameters is further reduced by describing each fit parameter with a low-order polynomial as a function of wavelength. The goal is to remove most of the flux from the faint companion; the quality of the

fit need not be very good. The SD technique is then applied to the data cube from which the faint companion light has been removed, to first order.

The result data cube will contain residual companion flux due to inaccuracies in the fit. However, as most of the PSF features will have been eliminated by the SD process, we can use the result data cube as a starting point for a second iteration, fitting the faint companion more accurately than in the initial step. After subtracting the improved estimate of the faint companion light from the observed data cube, we apply the SD method again (second iteration) to obtain an improved result cube. Further iterations are carried out until convergence is achieved, and the extracted spectrum of the faint companion does not change. Fit parameters such as companion position and width, fixed at first, can be free parameters in subsequent iterations to improve the quality of the fit. We applied this iterative technique to the data presented in the next section, and found that only two iterations were required to achieve convergence.

The key to successfully applying the iterative procedure is to produce a reasonable, if noisy, estimate of the faint companion flux in the first iteration. This can be achieved by subtracting an ideal Airy pattern centred on the primary, or by subtracting data taken with the same instrument, but with a different rotator angle. In either case, the purpose is to estimate and remove the azimuthally symmetric component of the PSF, so as to enhance the contrast at the location of the faint companion. This can also be achieved by fitting a radial profile to the primary's light distribution, and subtracting it from the observed data cube. The radial profile can also be used to model the flux distribution from the faint companion, resulting in a better subtraction of the companion flux in the data processing.

For faint companions located farther than the bifurcation point, applying the iterative procedure outlined above can still improve the S/N of the final extracted spectra, as it reduces the contamination from the faint companion light in the PSF estimate.

2.4 Optimizing the S/N of the extracted spectra

Observations carried out with a general-purpose AO system suffer from the added complication of moderate Strehl that varies substantially with wavelength. Consequently, the FWHM of the PSF does not scale with λ as expected for a purely diffraction-limited system. Instead, with Strehl increasing with wavelength, the PSF is too broad at the shortest wavelengths, and too narrow at the longest wavelengths, a feature which persists in the scaled data cube. This results in a radial distance and wavelength-dependent flux residual after applying the SD technique. Consequently, the continuum of the faint companion is incorrectly determined. To rectify these errors caused by the varying Strehl, we fit and subtract a radial profile for the primary light from each spectral channel of the data cube prior to applying the SD technique. The data presented in Section 3 have been so treated.

A further improvement in S/N of the extracted spectrum is obtained by scaling the PSF estimate cube back to the original observed pixel scale and subtracting it from the observed data cube, rather than scaling the observed data cube and performing the subtraction of the scaled cubes. Although the scaling is a linear operation, an interpolation is performed to place all scaled channels on a common grid, and this results in noise enhancement. As the observed data have much lower S/N (per spectral channel) than the PSF estimate formed by the SD technique, the noise enhancement is avoided almost completely by scaling and de-scaling the high-S/N PSF estimate rather than the lower S/N observed data cube.

3 DEMONSTRATION

We obtained observations of the local young K dwarf AB Doradus (AB Dor), which is known to have a M dwarf companion (AB Dor C) with $\Delta K = 5$ mag only 0.2 arcsec away (Close et al. 2005). AB Dor A has a K -band magnitude of 4.6, making it an ideal AO guide star. Details of the AB Dor C observations and data analysis are presented here as proof-of-concept of the proposed extensions to the SD technique, as described in previous sections. It is also the first time the SD method has been applied to a ground-based AO-assisted IFS data set, with moderate Strehl and no coronagraph present. As such, it also serves as an experimental verification of the SD method and its applicability to ground-based data sets. We also present a high-S/N H - and K -band spectrum of AB Dor C extracted using this technique. Further detailed analyses of the results of these observations are published in the companion paper by Close et al. (2007, hereafter Paper II).

3.1 Observations

Data were obtained on the nights of 2006 January 24 and 25 with the SINFONI instrument (Thatte et al. 1998; Eisenhauer et al. 2003; Bonnet et al. 2004) at the Cassegrain focus of the ESO VLT-UT4 (Yepun). Table 2 lists the observations, all with the H+K grating. DIT is the time per exposure, with N-DIT such exposures averaged together by the readout hardware to produce a single frame. The total exposure time is made of many such averaged frames. In addition to the AB Dor system, observations were made of a star in the Pleiades cluster to serve as an M8 template of young age, and of several telluric standards, at both 25- and 250-mas plate scales.

AB Dor A was used as the guide star for the SINFONI adaptive optics module (Bonnet et al. 2004). The mean Strehl ratio delivered was 0.37 on the 25th, and 0.35 on the 26th, as reported by the SINFONI AO system itself. SINFONI was used in the 25-mas scale to ensure adequate sampling of the PSF. To enable removal of bad pixels, and to sample SINFONI's rectangular spaxels, a dither pattern with offsets of exactly ± 0.5 spaxels was used. The H+K grating was used to maximize the wavelength coverage, resulting in a spectral resolving power of ~ 1500 , and instantaneous wavelength coverage of 1.4–2.45 μm . No blank-sky observations were taken for AB Dor at the 25 mas pixel scale, as it was clear that the data would be dominated by photon/speckle noise from AB Dor A. The J band was used for acquisition to avoid saturation of the detector array. Seeing during the observations (as reported by the Atmospheric Site Monitor) varied between 0.58 and 0.74 arcsec, with a mean of

Table 2. List of observations. All observations were made with the H+K grating. The 250-mas observations will not be discussed in this paper.

Target	Spaxel size (mas)	DIT (s)	N-DIT	Total exposure (s)
AB Dor ^a	25	5.0	16	1280
AB Dor ^b	25	5.0	16	1280
AB Dor ^c	250	0.83	4	6.64
Teide 1 ^d	250	300	1	600

^a – 16°5 PA.

^b + 16°5 PA.

^c These data were taken to bootstrap the spectral PSF from the 250-mas pixel scale to the 25-mas pixel scale, if required.

^d Full designation is Cl* Melotte 22 Teide 1, template of M8 spectral type.

0.64 arcsec on the 25th, and between 0.61 and 0.86 arcsec with a mean value of 0.69 arcsec on the 26th.

3.2 Data reduction

Basic data reduction followed the standard SINFONI data-reduction procedure, outlined in Schreiber et al. (2004) and Abuter et al. (2006), with extensions to deal with the 2K camera upgrade of 2005 February (Eisenhauer et al. 2002). The jitter pattern was corrected by combining data cubes, one for each on-source exposure recorded, creating a single mosaicked cube with a total observing time of 20 min for the data of the 25th, and a second one (with different rotator angle) for the data of the 26th. Accurate centroiding of AB Dor A in the resulting data cube showed a residual variation with wavelength, implying that the standard differential atmospheric refraction correction employed by the pipeline reduction was not accurate enough. Consequently, we disabled the differential atmospheric refraction correction in the standard reduction, and did a post-correction of the AB Dor A centroid movement along the wavelength axis of the data cube, using a cubic polynomial function. The resulting improved model for differential atmospheric refraction will be presented elsewhere.

It should be noted that even after disabling the differential atmospheric refraction correction, there are still three interpolations inherent in the production of a SINFONI data cube, two of which use a nearest neighbour interpolation algorithm with a tanh kernel, and one uses a polynomial interpolation algorithm. One interpolation is required to ‘straighten’ the spectra, a second does re-gridding on to an uniform grid in wavelength, and a third corrects for subpixel shifts between slices. We have not evaluated the impact of these interpolations in a quantitative manner, but it is likely that they do impact the maximum contrast achieved by these observations.

An implementation of the SD technique (and its extensions) used both IDL and GIPSY data analysis packages, in addition to the routines

from the SINFONI pipeline. GIPSY (Vogelaar & Terlouw 2001) was used primarily for visualization of the data cubes with sliceview, while most computationally intensive tasks were performed in IDL.

3.3 The SD technique and extensions

AB Dor C is located 0.2 arcsec from AB Dor A, at a PA of 181° at the epoch of these observations, based on orbit parameters determined by Nielsen et al. (2005). Using equation (3), we note that AB Dor C is closer than the bifurcation radius, thus requiring an iterative procedure to identify the companion and extract its spectrum.

The technique described in previous sections was applied to the AB Dor data cubes to extract a spectrum of the companion AB Dor C. As AB Dor C is clearly visible in the raw data cube (see Fig. 2), there was no problem in determining the companion location. However, AB Dor C did overlap with a bright spot in the diffraction pattern in the data taken on the 25th. The pattern of four bright spots is caused by the telescope secondary mount diffraction pattern superposed on the Airy pattern. Consequently, an accurate determination of the companion location did require a second iteration of the SD technique, as explained in Section 2.3 above. Due to the strong dip in atmospheric transmission at the edges of both *H* and *K* bands, the processing was confined to wavelength ranges 1.457–1.80 and 1.95–2.45 μm , respectively, for the *H* and *K* bands. A total of two iterations were needed for the SD technique to yield a high-S/N PSF estimate free from companion flux.

3.4 Results

Fig. 2 shows one wavelength slice of the SINFONI IFS data cube for the AB Dor system before and after the application of the SD technique (and its extensions) described above. The separation of AB Dor C from the parent was only 0.2 arcsec at this epoch, while

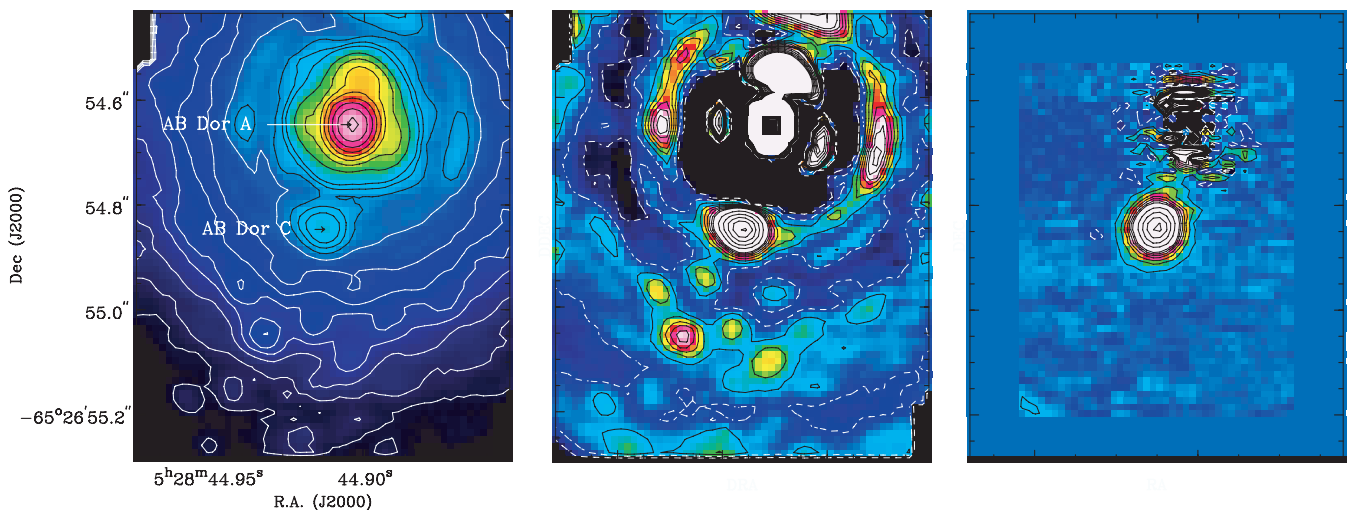


Figure 2. Illustration showing the efficacy of the SD technique at removing both PSF artefacts and super-speckles from the SINFONI IFS data cube for the AB Dor system. The left-hand frame shows one wavelength slice of the observed data cube at 2.2 μm . Note that the entire vertical extent of the image is only 0.9 arcsec. The colour table is logarithmic (minimum 10^1 , maximum 10^4). The contours are logarithmic, from 0.9 to 2.3 in steps of 0.1, and from 2.3 to 4.0 in steps of 0.2. The middle frame shows the same data, but with a radial profile fitted and subtracted, so as to highlight the PSF imperfections. The super-speckles are easily confused with real sources in this narrow-band image. The colour table is now linear (minimum -10 , maximum 25), with contours from -12.5 to 32.5 in steps of 5, and from 32.5 to 150 in steps of 20. The four-fold symmetry of the Airy pattern arises from the superposition of the diffraction spikes of the secondary support structure on the Airy rings. The right-hand frame shows the same wavelength slice of the data cube, after applying the SD technique iteratively. Colour table and contours are the same as for the middle frame. Super-speckles are completely absent at the lowest contour level of ± 2.5 , corresponding to a 1σ error of ≤ 1 unit.

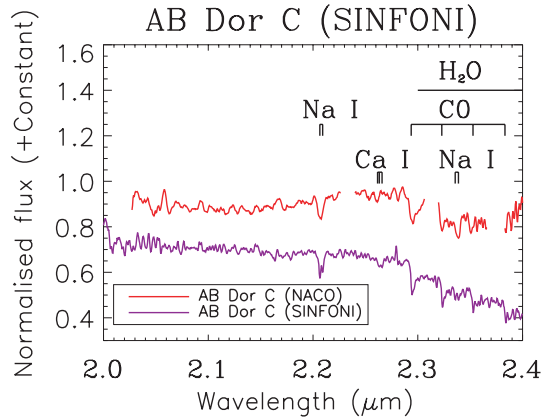


Figure 3. The K -band extracted spectrum of AB Dor C, with some of the prominent stellar features marked. The K -band spectrum obtained by NACO AO long-slit spectroscopy, at 0.150 arcsec separation (Nielsen et al. 2005) is also shown for comparison. Note that our spectrum also correctly recovers the continuum slope, vital for deriving the spectral type of this young object (see Paper II for details of the spectral classification). The ‘emission’ feature just shortward of the first CO bandhead is a residual telluric feature that was not correctly subtracted out.

the flux contrast was $\Delta m = 4.90$. The left-hand frame shows the raw data, while the central frame has a smooth radial profile fitted and subtracted from the raw data to highlight the PSF artefacts, and in particular, the super-speckles. The right-hand frame shows the result of applying the technique described in Section 2. We can successfully remove both Airy pattern residuals, as well as super-speckles. Note the four-fold symmetry of the Airy pattern, a result of the superposition of the Airy ring with the diffraction from the spider arms of the secondary. Unfortunately, AB Dor C is located at the same orientation as one of the Airy peaks. We prefer to use this data set as it has significantly better Strehl, although the other data set (rotated by 33°) places AB Dor C at a more favourable location relative to the Airy peaks. Stepping through the data cube along the wavelength axis, all PSF imperfections scale linearly with wavelength,² while the real object stays at a fixed location. The data do demonstrate that the SD technique can effectively separate companion and PSF contributions, even if they are spatially coincident in a single wavelength channel. The removal of the super-speckles is of particular value, as their shape mimics point sources in the field in any narrow-band image.

3.4.1 Extracted spectra of AB Dor C

Figs 3 and 4 show the normalized, extracted spectra of AB Dor C, using the SD technique. The data have been smoothed with a boxcar of width 3 pixel, corresponding to 1.5 nm. The S/N of the K -band spectrum exceeds 40, as derived from the contrast values discussed in Section 3.4.2. The quality of the spectrum is limited by systematic errors in the division of telluric features, as no sky observations were performed. The NACO spectrum previously obtained by Close et al. (2005) at a tighter 0.15-arcsec separation is also shown for comparison. Note that the SD technique is able to reproduce not only the spectral features but also the continuum slope, in contrast to AO long-slit measurements with varying slit filling

² mpeg movies of the raw, radial profile subtracted and SD result data cubes can be viewed at <http://www-astro.physics.ox.ac.uk/~thatte/abdorc>.

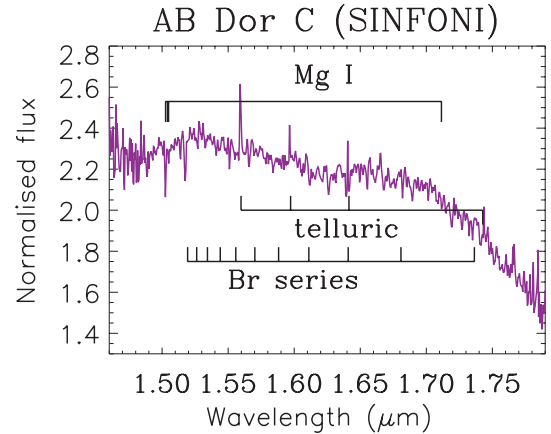


Figure 4. The H -band extracted spectrum of AB Dor C, with some of the stellar features marked. Also marked are the locations of the Brackett series hydrogen recombination lines, as these were present in absorption in the late B telluric standard. Although every effort was taken to accurately fit these lines, some residuals remain. As no sky observations were made, some of the brightest night sky OH emission lines are also present in the derived spectrum. The H and K spectra were obtained simultaneously, by applying the SD technique (and its extensions) to the data cube covering both H and K bands. They are shown separately for clarity.

factors. The output data cube, after applying the SD technique, is used to measure the position, flux, and spectral type of AB Dor C. At the epoch of these observations, AB Dor C was located 201.7 ± 10 milliarcsec from AB Dor A, at a PA of $180^\circ.78$. The K magnitude was 4.90 mag fainter than AB Dor A, which, combined with the 2MASS measurement for AB Dor A yields $K = 9.59$ for AB Dor C. A spectral type of $M5.5 \pm 0.5$ can be derived by comparing the observed spectrum with young and old templates. A detailed analysis of the properties of AB Dor C (including its spectral-type determination) is presented in Paper II. Note that both the companion flux and its spectral continuum slope are correctly derived using the iterative method described in Section 2.3 above.

3.4.2 Achieved contrast

The remarkable success of the SD technique at removing light contamination resulting from PSF imperfections is illustrated in Fig. 5. The plot shows the resulting radial profile for a 20 min exposure of the AB Dor system observed with SINFONI, with a spectral width of 5.5 nm, using the SD technique. AB Dor C is clearly visible as a bump in the radial profile at 0.2 arcsec. The curve shows that the contrast achieved (1σ) is ~ 9 mag at 0.2 arcsec, and 11 mag at 0.5 arcsec, without using a coronagraph. Note that the effective spectral resolution ($R = 400$) is higher than that achieved by SDI ($R = 50$) (Lenzen et al. 2004; Biller et al. 2006). The achieved contrast is still ~ 1 mag from the photon noise limit, although we suspect that some residual noise is attributable to non-optimal interpolations in the data-reduction procedure, and can be improved upon. The ultimate limitations of the technique will be addressed in a separate paper.

3.5 Faint object detection

AB Dor C is only 5 mag fainter than AB Dor A, and could thus be easily detected in the raw data cube. However, we note that the SD technique can also be used for detection of faint companions.

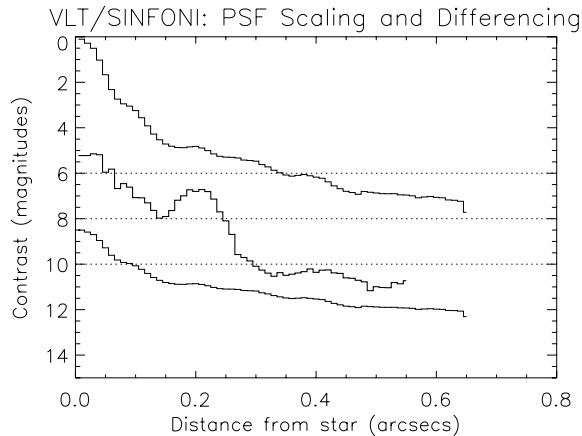


Figure 5. The plot shows three curves – the top curve is the radial profile of AB Dor A. The bottom curve is the square root of the top curve, so it represents the photon noise limit. The middle curve is the standard deviation in the SD result frame, so it is a measure of the residual noise. The horizontal lines at 6, 8 and 10 mag are for reference. The large bump at 0.2 arcsec in the SD result frame is due to AB Dor C. The achieved contrast is 9 mag at 0.2 arcsec, and 11 mag at 0.5 arcsec, in 20 min exposure time at $R_{\text{eff}} = 400$. As no coronagraph is used, very high contrasts can be obtained at small inner working radii.

Any feature whose radial distance from the primary does not scale with wavelength generates a radial streak in a collapsed image created by averaging the scaled data cube along the spectral dimension. Subtracting the collapsed image (scaled back appropriately for each wavelength) from the original data cube results in a diminished companion flux plus an inward negative streak at the shortest wavelengths, a diminished flux companion plus a symmetric negative radial streak at central wavelengths, and a weaker companion plus an outward negative streak at the longest wavelengths. The final collapsed image shows the characteristic pattern of a positive object sitting atop a long negative radial streak centred on the object (see both ‘planets’ in fig. 26 of Sparks & Ford 2002). This characteristic pattern can be used to detect faint companions. Furthermore, if the primary’s radial light profile is fitted and subtracted from each wavelength slice of the data cube prior to applying the SD technique, the contrast of the faint companion can be further enhanced.

If the technique is applied to data cubes taken at two different rotator angles and subtracted from each other prior to step 1, only features that are stationary on the sky will remain. In addition to showing the characteristic pattern described above, they will also show a positive and negative image of true celestial objects, separated by the difference in rotator angles. The resulting pattern can be easily used to identify potential faint companions.

4 CONCLUSIONS

In this paper, we have introduced extensions to the SD technique proposed by Sparks & Ford (2002) for achieving high-contrast imaging spectroscopy with an AO-fed IFS at small inner working radii. Applying this technique to real data, we have shown it to provide very high contrast spectra of faint companions very close to bright stars. The achieved contrast is substantially better than previously achieved by other techniques, especially as no coronagraph was used. The absence of a coronagraph removes limits on the smallest inner working radius, especially valuable as most exoplanet candidates are expected to lie at very small separations from the parent

star. The SD technique holds great promise for direct imaging of exoplanets, as it simultaneously detects and spectrally characterizes any faint companion, thus removing the need for expensive and time-consuming follow-up observations, either to detect common proper motion or to obtain a spectrum of the faint companion. In addition, the technique does not require any assumptions about the companion’s spectral characteristics (e.g. presence of a CH_4 feature), and can therefore be applied to any high-contrast application.

Our demonstration of the efficacy of the SD technique to obtain spectra of the close-in faint companion AB Dor C shows that image slicer based IFSs are capable of achieving very high contrasts, contrary to the expectations of several groups (Claudi et al. 2004; Berton et al. 2006; Verinaud et al. 2006) who were concerned that large non-common-path errors would limit the contrast achievable with these systems. The SINFONI IFS design (Tecza et al. 2000, 2003) exclusively uses classically polished flat glass mirrors in its image slicer, thus achieving very small non-common-path errors, as demonstrated here. Indeed, we have shown that an IFS alone can provide a large fraction of the total contrast requirement of an exoplanet direct detection instrument.

A successful application of the SD technique requires large instantaneous wavelength coverage, strongly favouring image slicer based IFS designs. These naturally provide large simultaneous wavelength coverage, while it is rather difficult to achieve a large bandwidth in lenslet array based designs. The requirement to keep non-common-path errors to an absolute minimum strongly favours image slicer designs with classically polished glass slicing optics (not just slicing mirrors, but the entire slicer optics), as implemented in the SINFONI spectrograph (Tecza et al. 2000, 2003).

ACKNOWLEDGMENTS

We thank the ESO Director General for allocating Director’s discretionary time to carry out these observations. We thank MPE for use of the SPRED SINFONI data-reduction software. This paper is based on observations collected at ESO, Chile under ESO programme ID 276.C-5013. NT, FJC and MT are funded through Marie-Curie Excellence Grant MEXT-CT-2003-002792. ELN is supported by a Michelson Fellowship. LMC is supported by an NSF CAREER award and the NASA Origins of Solar Systems programme. We thank the referee, W. B. Sparks, for extensive comments that greatly improved this paper.

REFERENCES

- Abuter R., Eisenhauer F., Schreiber J., Horrobin M., Genzel R., Davies R., Lehnert M., Tecza M., 2006, *New Astron. Rev.*, 50, 398
- Berton A., Feldt M., Gratton R., Hippler S., Henning T., 2006, *New Astron. Rev.*, 49, 661
- Berton A., Gratton R. G., Feldt M., Henning T., Desidera S., Turatto M., Schmid H. M., Waters R., 2006, *PASP*, 118, 846
- Beuzit J. L. et al., 2006, in Arnold L., Bouchy F., Moutou C., eds, *Tenth Anniversary of 51 Peg-b: Status of and Prospects for Hot Jupiter Studies*. Frontier Group, Paris, p. 353
- Biller B. A., Close L. M., Lenzen R., Brandner W., McCarthy D., Nielsen E., Kellner S., Hartung M., 2006, in Aime C., Vakili F., eds, *Proc. IAU Coll. 200, Direct Imaging of Exoplanets: Science & Techniques*. Cambridge Univ. Press, Cambridge, p. 571
- Bonnet H., Abuter R., Baker A., Bornemann W., Brown A., Castillo R., Conzelmann R., Damster R., 2004, *The Messenger*, 117, 17
- Bonnet H. et al., 2004, in Bonaccini C. D., Ellerbroek B. L., Ragazzoni R., eds, *Proc. SPIE Vol. 5490, Advancements in Adaptive Optics*. SPIE, Bellingham, p. 130 (doi:10.1117/12.551187)

- Burrows A., Sudarsky D., Hubeny I., 2004, *ApJ*, 609, 407
- Claudi R. U., Turatto M., Gratton R., Antichi J., Buson S., Pernechele C., Desidera S., Baruffolo A., 2004, in Moorwood A. F. M., Iye M., eds, *Proc. SPIE Vol. 5492, Ground-based Instrumentation for Astronomy*. SPIE, Bellingham, p. 1351 (doi:10.1117/12.551427)
- Close L. M. et al., 2005, *Nat*, 433, 286
- Close L. M., Thatte N., Neilson E. L., Abuter R., Clarke F. J., Tecza T., 2007, *ApJ*, in press (astro-ph/0703564) (Paper II)
- Eisenhauer F. et al., 2003, in Iye M., Moorwood A. F. M., eds, *Proc. SPIE Vol. 4841, Instrument Design and Performance for Optical/Infrared Ground-based Telescopes*. SPIE, Bellingham, p. 1548
- Eisenhauer F., van der Werf P., Thatte N., de Zeeuw T., Tecza M., Franx M., Iserlohe C., 2002, in Bergeron J., Monnet G., eds, *Proc. ESO Workshop, Scientific Drivers for ESO Future VLT/VLTI Instrumentation*. Springer-Verlag, Berlin, p. 149 (doi:10.1007/10857019_22)
- Fusco T., Rousset G., Beuzit J.-L., Mouillet D., Dohlen K., Conan R., Petit C., Montagnier G., 2005, in Grycewicz T. J., Marshall C. J., eds, *Proc. SPIE Vol. 5903, Focal Plane Arrays for Space Telescopes II*. SPIE, Bellingham, p. 148 (doi:10.1117/12.616518)
- Guyon O., 2004, in Domenico B. C., Brent L. E., Roberto R., eds, *Proc. SPIE Vol. 5490, Advancements in Adaptive Optics*. SPIE, Bellingham, p. 593 (doi:10.1117/12.552421)
- Lenzen R., Close L., Brandner W., Biller B., Hartung M., 2004, in Moorwood A. F. M., Masanori I., eds, *Proc. SPIE Vol. 5492, Ground-based Instrumentation for Astronomy*. SPIE, Bellingham, p. 970 (doi:10.1117/12.549406)
- Macintosh B. A., Bauman B., Wilhelmsen Evans J., Graham J. R., Lockwood C., Poyneer L., Dillon D., 2004, in Bonaccini Calia D., Ellerbroek B. L., Ragazzoni R., eds, *Proc. SPIE Vol. 5490, Advancements in Adaptive Optics*. SPIE, Bellingham, p. 359 (doi:10.1117/12.552188)
- Marois C., Racine R., Doyon R., Lafrenière D., Nadeau D., 2004, *ApJ*, 615, L61
- Marois C., Doyon R., Nadeau D., Racine R., Riopel M., Vallée P., Lafrenière D., 2005, *PASP*, 117, 745
- Marois C., Lafrenière D., Doyon R., Macintosh B., Nadeau D., 2006, *ApJ*, 641, 556
- Nielsen E. L., Close L. M., Guirado J. C., Biller B. A., Lenzen R., Brandner W., Hartung M., Lidman C., 2005, *Astron. Nachr.*, 326, 1033
- Racine R., Walker G. A. H., Nadeau D., Doyon R., Marois C., 1999, *PASP*, 111, 587
- Ren D., Wang H., 2006, *ApJ*, 640, 530
- Schreiber J., Thatte N., Eisenhauer F., Tecza M., Abuter R., Horrobin M., 2004, in Ochsenbein F., Allen M. G., Egret D., eds, *ASP Conf. Ser. Vol. 314, Astronomical Data Analysis Software and Systems XIII*. Astron. Soc. Pac., San Francisco, p. 380
- Soummer R., Aime C., Ferrari A., Sivaramakrishnan A., Oppenheimer B. R., Makidon R., Macintosh B., 2006, in Aime C., Vakili F., eds, *Proc. IAU Coll. 200, Direct Imaging of Exoplanets: Science & Techniques*. Cambridge Univ. Press, Cambridge, p. 367
- Sparks W. B., Ford H. C., 2002, *ApJ*, 578, 543
- Tecza M., Eisenhauer F., Iserlohe C., Thatte N. A., Abuter R., Roehrl C., Schreiber J., 2003, in Atad-Ettdgui E., D'Odorico S., eds, *Proc. SPIE Vol. 4842, Specialized Optical Developments in Astronomy*. SPIE, Bellingham, p. 375
- Tecza M., Thatte N. A., Eisenhauer F., Mengel S., Roehrl C., Bickert K., 2000, in Iye M., Moorwood A. F., eds, *Proc. SPIE Vol. 4008, Optical and IR Telescope Instrumentation and Detectors*. SPIE, Bellingham, p. 1344
- Thatte N. A. et al., 1998, in Bonaccini D., Tyson R. K., eds, *Proc. SPIE Vol. 3353, Adaptive Optical System Technologies*. SPIE, Bellingham, p. 704
- Verinaud C. et al., 2006, in Aime C., Vakili F., eds, *Proc. IAU Coll. 200, Direct Imaging of Exoplanets: Science & Techniques*. Cambridge Univ. Press, Cambridge, p. 507
- Vogelaar M. G. R., Terlouw J. P., 2001, in Harnden F. R., Jr, Primini F. A., Payne H. E., eds, *ASP Conf. Ser. Vol. 238, Astronomical Data Analysis Software and Systems X*. Astron. Soc. Pac., San Francisco, p. 358

This paper has been typeset from a $\text{\TeX}/\text{\LaTeX}$ file prepared by the author.